Ephaptic Interactions in the Mammalian Olfactory System

Hemant Bokil, Nora Laaris, Karen Blinder, Mathew Ennis, and Asaf Keller

Department of Anatomy and Neurobiology, Program in Neuroscience, University of Maryland, Baltimore, Maryland 21201

Ephaptic coupling refers to interactions between neurons mediated by current flow through the extracellular space. Ephaptic interactions between axons are considered negligible, because of the relatively large extracellular space and the layers of myelin that separate most axons. By contrast, olfactory nerve axons are unmyelinated and arranged in tightly packed bundles, features that may enhance ephaptic coupling. We tested the hypothesis that ephaptic interactions occur in the mammalian olfactory nerve with the use of a computational approach. Numerical solutions of models of axon fascicles show that significant ephaptic interactions occur for a range of physiologically relevant parameters. An action potential in a single axon can evoke action potentials in all other axons in the fascicle. Ephaptic interactions can also lead to synchronized firing of independently stimulated axons. Our findings suggest that ephaptic interactions may be significant determinants of the olfactory code and that such interactions may occur in other, similarly organized axonal or dendritic bundles.

Key words: volume conduction; nonsynaptic interactions; olfactory bulb; olfactory nerve; unmyelinated axons; olfactory coding

Ephaptic coupling is the process by which neighboring neurons affect each other by current spread through the extracellular space. The prevailing view is that in most mammalian nervous tissues, ephaptic interactions are negligible and can therefore be ignored (Segundo, 1986). For example, ephaptic interactions among axons are constrained by the low resistance of the relatively large extracellular space separating most axons and by the insulating myelin sheath surrounding each axon. As the extracellular space increases, its resistance decreases and voltage gradients in the extracellular space rapidly dissipate. Therefore, the extracellular space is typically considered to have zero resistance and its potential is ignored. As a result, neighboring axons are thought not to affect each other via ephaptic interactions (Esplin, 1962; Barr and Plonsey, 1992).

However, in several brain regions axons are arranged in configurations that may favor ephaptic interactions. One example is the axons contained within the mammalian olfactory nerve, which originate in the olfactory epithelium and project to the main olfactory bulb. These axons lack myelin, and they are arranged in densely packed fascicles (Doucette, 1984; Datson et al., 1990; Griff et al., 2000). Each fascicle contains between 10 and 200 axons (Marín-Padilla and Amieva, 1989), with each axon having a diameter of $\sim$0.2 μm (Griff et al., 2000). Axons within a fascicle are oriented parallel to each other, and do not branch before they reach their termination site in the glomeruli of the olfactory bulb (Moran et al., 1982; Datson et al., 1990). The high packing density and the geometry of these axons suggest that neighboring axons can influence each other through ephaptic interactions. Here, we test the hypothesis that ephaptic interactions occur between olfactory axons with the use of computational models.

Parts of these results have been published previously in abstract form (Bokil et al., 2001).

MATERIALS AND METHODS

Computational approaches. The rationale and approaches used for constructing the two cable models used in this study are described in detail in Results. The Appendix includes additional descriptions of more technical aspects of these computational models.

Electron microscopy. Adult (>45 d old) male rats were deeply anesthetized and transcardially perfused with a buffered aldehyde solution containing 0.5% paraformaldehyde and 2.5% glutaraldehyde. The olfactory bulbs were removed, and coronal sections through the bulb were prepared for standard transmission electron microscopy. Photomicrographs were printed at a final magnification of 72,000× and used for morphometric analyses of axonal diameters and intracellular and extracellular spaces, performed with the Neurolucida (MicroBrightField, Colchester, VT) morphometry system.

RESULTS

Mean field model: passive axons

The degree of ephaptic coupling between neighboring axons is determined by the interplay between the extracellular resistance and the intracellular and membrane resistance of the axons. The geometry of olfactory nerve axons suggests that it is useful to distinguish between longitudinal and transverse extracellular re-

Received April 20, 2001; revised July 23, 2001; accepted July 26, 2001.

This work was supported by United States Public Health Service (USPHS) Grants NS-31078 (A.K.), DC-00347, and DC-03915 (M.E.). H.B. and K.B. are supported by USPHS training Grant DC-00054. We thank Drs. John Rinzel and Larry Cohen for their assistance and critical discussions. We also thank Drs. Greg Carlson, Michael Shipley, and Dan Tranchina for their helpful comments.

Correspondence should be addressed to Dr. Asaf Keller, Department of Anatomy and Neurobiology, University of Maryland School of Medicine, 685 West Baltimore Street, Baltimore, MD 21201. E-mail: akeller@umaryland.edu.

Dr. Bokil's present address: Bell Laboratories, Room 1D-367, 600 Mountain Avenue, Murray Hill, NJ 07974.

This article is published in *The Journal of Neuroscience*, Rapid Communications Section, which publishes brief, peer-reviewed papers online, not in print. Rapid Communications are posted online approximately one month earlier than they would appear if printed. They are listed in the Table of Contents of the next open issue of JNeurosci. Cite this article as: JNeurosci, 2001, 21:RC173 (1–5). The publication date is the date of posting online at www.jneurosci.org.

http://www.jneurosci.org/cgi/content/full/5719

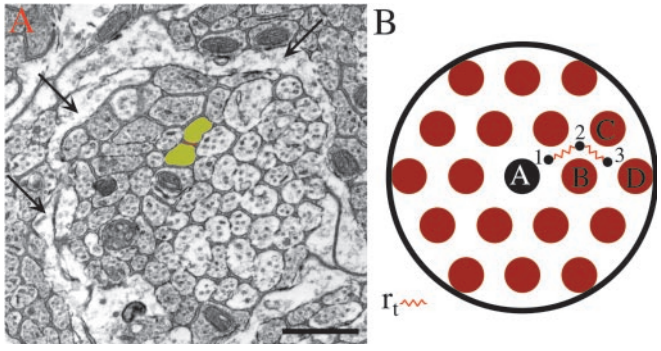

Figure 1. *A*, An electron micrograph of a coronal section through the olfactory nerve layer, depicting a fascicle of axons (2 axons are marked in *yellow*, and the intervening extracellular space in *red*), surrounded by glial processes (*arrows*). Scale bar, 0.5 μm. *B*, A schematic of a cross section of a fascicle of 19 axons arranged in a triangular lattice. This schematic is the basis for the geometric model described in the text. Shown are the central, stimulated axon (*A*), three of its neighbors (*B–D*), connected through extracellular cables (*1–3*) situated on the interstitial sites of the lattice; following symmetry arguments, these are the only axons that need to be considered in the calculations.

sistances. For axons with diameter d, the intracellular resistance per unit length $r_i = 4R_i/(\pi d^2)$, and the membrane resistance per unit length $r_m = R_m/(\pi d)$, where R_i (Ωcm) is the cytoplasmic resistivity and R_m (Ωcm^2) is the specific membrane resistance. Denoting the ratio of the extracellular to intracellular cross-sectional areas by β (mean ± SEM = 0.047 ± 0.001; $n = 7$) (Fig 1*A*), the longitudinal extracellular resistance per unit length $r_e = r_i/(N\beta)$, where N is the number of axons in a fascicle. Because the transverse resistance per unit length is $r_t \ll r_m$, we assume that each transverse cross section of the extracellular space is equipotential, i.e., $r_t = 0$ (see Appendix). This suggests the following mean-field model: we consider N axons in a fascicle, model them as one-dimensional cables along the x-axis, and assume that only a single axon (axon A) is stimulated. Then, the remaining N-1 axons will have the same membrane potential. Denoting the membrane potentials of A and the remaining axons by V^A and V^B, standard cable theory (see Appendix) leads to the following equations:

$$c_m \frac{\partial V^A}{\partial t} = \frac{a_{11}}{D}\frac{\partial^2 V^A}{\partial x^2} - \frac{a_{12}}{D}\frac{\partial^2 V^B}{\partial x^2} - I^A_{ion} + I_{stim},$$

$$c_m \frac{\partial V^B}{\partial t} = -\frac{a_{21}}{D}\frac{\partial^2 V^A}{\partial x^2} + \frac{a_{22}}{D}\frac{\partial^2 V^B}{\partial x^2} - I^B_{ion},$$

where c_m (μF/cm) is the membrane capacitance per unit length, $I^{A,B}_{ion}$ denotes the membrane currents, and I_{stim} is the stimulating current. Finally, $a_{11} = r_i + r_e(N-1)$, $a_{12} = r_e(N-1)$, $a_{21} = r_e$, $a_{22} = r_i + r_e$, and $D = r_i^2 + Nr_ir_e$. Note that the above equations can be written in terms of dimensionless variables, implying that they apply to axons of arbitrary diameter. However, in the subsequent discussion, we will frame the analysis in the context of olfactory nerve axons having a measured diameter in the olfactory nerve layer of 0.2 ± 0.05 μm ($n = 325$) (Fig. 1).

We first consider the case in which the axons are electrotonically passive, that is, they have no voltage-dependent conductances, and in particular consider the steady-state solutions to the above equations for a constant depolarizing current into axon A ($I_{stim} = I\delta(x)$). Figure 2*A* shows the coupling coefficient, defined as the ratio $V^B(x = 0)/V^A(x = 0)$, as a function of β for different

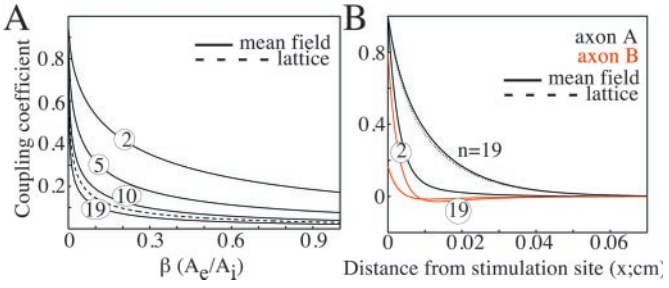

Figure 2. Coupling in axons having only passive membrane properties. *A* shows the effect of varying the ratio of extracellular to intracellular space (β) on the degree of coupling (coupling coefficient, V^A_m/V^B_m) for different values of N, computed for the mean-field and geometric model shown in Figure 1*B*. *B* shows the spatial profile of membrane potentials in a fascicle of N axons ($\beta = 0.05$), after a DC current injection across the membrane of axon A at $x = 0$. Here, $r = 100$ Ωcm, and $R_m = 3333$ Ωcm^2.

values of N. Figure 2*B* shows the spatial profile of V^A and V^B for $N = 2$ and 20 at $\beta = 0.05$. As evidenced from these Figures, the coupling coefficient is highly sensitive to both the ratio of extracellular to intracellular spaces (β) and the number of axons in a fascicle (N). For β values measured for the olfactory nerve (0.05), these analyses predict that significant ephaptic interactions occur in small- to medium-size fascicles.

Geometric model

Because the mean-field model ignores the spatial relationships between the axons and thereby underestimates potential interactions between nearest-neighbors, we tested its predictions against a second, geometric model. We consider nineteen axons in a triangular lattice (Fig. 1*B*) and model the extracellular space as 24 one-dimensional cables situated on the interstitial sites of the lattice, each with longitudinal resistance $24r_e$ per unit length. Unlike the mean-field model, here adjacent extracellular cables are connected through transverse resistances $r_t = 10\ R_i$ per unit length (see Appendix). With only the central axon A stimulated (Fig. 1*B*), we solved the resulting cable equations in the steady state. We found that axons B, C, D had nearly identical and isotropic membrane potentials, with values that agree with results of the mean-field calculation (Fig. 2*A*,*B*). This shows that the mean-field model is a good approximation, the conclusion being insensitive to the precise value of r_t; the results are virtually identical for r_t as large as 10,000 R_i. For both the mean-field and geometric models, we set $R_i = 100$ Ωcm and $R_m = 3333$ Ωcm^2; the coupling coefficient is unaffected by the choice of these parameters.

Axons with active membrane properties

The preceding analyses focused on axons having only passive membrane properties. Exploring spiking activity requires consideration of active membrane conductances. Because these conductances have not been characterized for mammalian olfactory nerve axons, we chose voltage-gated sodium and potassium channels with standard Hodgkin–Huxley membrane parameters in the mean-field model, and integrated the resulting equations (see Appendix) with the forward Euler method (Press et al., 1992). When $N = 2$ and axon A is stimulated to evoke a single action potential, a propagating action potential is initiated simultaneously in axon B at a site directly opposite the site of stimulation ($\beta = 0.05$) (Fig. 3*A*). Thus, consistent with the predictions of the passive models above, ephaptic interactions can evoke action potentials in neighboring axons. To ensure that this result was not

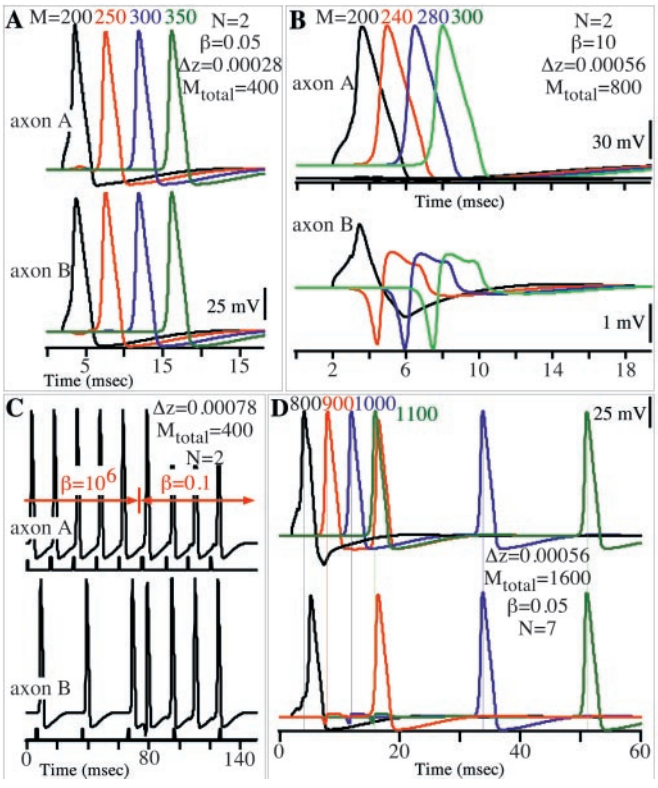

Figure 3. Coupling in axons with active membrane properties. When $\beta = 0.05$, a single action potential evoked in axon A induces a propagating action potential in axon B (*A*). When $\beta = 10$, a subthreshold, propagating potential is evoked in axon B (*B*). *M* denotes the compartment number in the 400-compartment cable model; stimulation site is $M = 200$ for both *A* and *B*. *C*, In the absence of ephaptic coupling ($\beta = 1{,}000{,}000$), different trains of current pulses injected into each axon result in repetitive firing at different frequencies. Enabling ephaptic coupling ($\beta = 0.1$) at $t = 75$ msec results in synchronous firing in both axons. *D*, The difference in propagation velocities between the two axons results in the unstimulated axons inducing a feedback action potential in the stimulated axon, after which the system becomes phase-locked.

attributable to the choice of specific Hodgkin–Huxley conductances, we verified that reducing the sodium conductance by up to 50% or increasing it by 200% did not affect this result qualitatively; a single action potential in one axon led to a single action potential in its neighbor.

By comparison, when β is large, the membrane potential of axon(s) B remains subthreshold ($\beta = 10.0$) (Fig. 3*B*). However, because this subthreshold waveform is induced by an action potential propagating along axon A, it too propagates along axon B at the same velocity as the action potential in A. When the number of axons in the fascicle (N) is larger, we find that there are two possible behaviors. For a large enough N ($N > 7$ at $\beta = 0.05$), the depolarization induced in unstimulated axons is subthreshold, with the behavior similar to that seen in Figure 3*B*. By contrast, for $2 < N < 8$, there is a delay in the onset of the action potentials in the unstimulated axons ($N = 7$) (Fig. 3*D*). Furthermore, the initial conduction velocity in the unstimulated axons is lower than that in *A*, with the action potential in the unstimulated axons preceded by a subthreshold propagating waveform. Consequently, an action potential is reinitiated in *A* after a refractory period, and the action potentials in the two axons are subsequently phase-locked (Fig. 3*D*). These effects are related to the relationship between the timing of action potentials and refractory periods in the different axons.

Previous studies suggested that interaxonal interactions may be mediated also by increases in extracellular K^+ concentrations (Malenka et al., 1981; Eng and Kocsis, 1987; Poolos et al., 1987). However, because these K^+-mediated effects only occur after trains of action potentials (Bliss and Rosenberg, 1979; Eng and Kocsis, 1987), they are unlikely to confound the present data, obtained in response to single stimulus pulses. The potential contribution of K^+-mediated interactions during trains of action potentials will be explored in future computational and experimental studies.

Like other sensory afferents, olfactory neurons are thought to code olfactory stimuli in the frequency of their action potentials (Duchamp-Viret et al., 2000). Reasoning that ephaptic interactions may affect the firing patterns in axons that begin firing at different frequencies, we evoked action potentials at different frequencies in two axons by a sequence of independent step current injections (Fig. 3*C*). When the axons were uncoupled ($\beta = 1{,}000{,}000$), axon A fired at a frequency of 66 Hz, and axon B fired at 33 Hz. When the axons were then coupled (by setting $\beta = 0.1$), both axons synchronized their firing at 66 Hz. Thus, these simulations predict that ephaptic coupling can synchronize the firing frequency of neighboring axons and that this synchrony can be entrained at high frequencies of firing.

Simultaneously active axons

Our analyses of ephaptic interactions in both the passive and active cases were thus far restricted to models in which only a single axon was stimulated. However, during olfactory discrimination, multiple axons in a fascicle are likely to be coactivated, and therefore our results thus far are likely to underestimate the efficacy of ephaptic interactions. To address this possibility, we evaluated the consequence of simultaneously stimulating a number of axons in a fascicle, with the use of the mean-field model described above.

Consider a fascicle of N axons with N_s of them identically stimulated. Because the interaction between the axons is mediated through the extracellular space that is equipotential in transverse cross section, the N_s stimulated axons have identical membrane potentials that we denote by V^A, and $(N - N_s)$ unstimulated axons have identical membrane potentials, which we denote by V^B. Then, the mean-field equations given above apply to this case with the coefficients a_{11}, a_{12}, a_{21}, $a_2 2$ now given by $r_i + r_e(N - N_s)$, $r_e(N - N_s)$, $N_s r_e$, $r_i + N_s r_e$ (see Appendix). Because r_e is inversely proportional to N, the equations (and their solutions) depend on N_s and N only through the ratio N_s/N, implying that the results for this case can be deduced from the results shown in Figures 2 and 3. For example, the results of the passive case for arbitrary N_s and N with $N_s/N = 1/19$ are identical to those shown in Figure 2 for $N = 19$. Similarly, the results for the active case for arbitrary N_s and N with $N_s/N = 1/7$ are identical to those shown in Figure 3*D* for $N = 7$. Thus, for example, in a fascicle of 200 axons, synchronous activation of more than one-seventh of the axons ($N_s > 28$) would lead to action potentials in all axons within that fascicle.

DISCUSSION

Our analyses reveal that, for a range of anatomically and physiologically relevant parameters, significant ephaptic coupling can occur between olfactory nerve axons. For example, for $\beta = 0.05$ (the ratio of extracellular to intracellular space measured here) (Fig. 1) the coupling coefficient is ~0.29 for a fascicle of 10 axons, suggesting that a 100 mV action potential in axon A would

produce a 29 mV depolarization in all other axons in the fascicle, which could be sufficient to initiate an action potential. Indeed, inclusion of active conductances in the models supports the prediction that action potentials in a single axons can evoke firing in its neighbors. Significantly, the predictions of both models are independent of the choice of biophysical membrane and extracellular parameters.

Both the mean-field and geometric models demonstrate that the coupling coefficient decreases inversely with β and N. Thus, the degree of ephaptic coupling is determined not only by the ratio of extracellular to intracellular spaces (β), but also by the absolute extracellular volume, which increases with N. Thus, ephaptic interactions are expected to be attenuated in larger fascicles. However, our results also reveal that simultaneous activation of multiple axons can lead to significant ephaptic coupling, even in large fascicles. Furthermore, even subthreshold ephaptic interactions may have significant effects on olfactory processing, by regulating the excitability of neighboring axons. Finally, if some aspects of olfactory coding are mediated by subthreshold potentials in olfactory axons (Pearce et al., 2001), ephaptic interactions are expected to have even more significant consequences for olfactory coding.

We demonstrated above that ephaptic interactions can evoke action potentials in axons neighboring an active axon independently of the specific Hodgkin–Huxley conductances selected for the model. Indeed, this conclusion can be deduced from the results of simulations of the passive case (Fig. 2), which demonstrate that ephaptic interactions can evoke large depolarizations in neighboring axons.

Functional implications

As they emerge from the olfactory epithelium, axons belonging to neighboring neurons, which respond to different odors (Ma and Shepherd, 2000) coalesce to form fascicles containing 10 to 20 axons (Marín-Padilla and Amieva, 1989). Our results suggest that activation of a subpopulation of the axons in these small fascicles may, via ephaptic interactions, result in coactivation of all the axons in that fascicle. These action potentials may back-propagate to the parent somata of these axons and affect the ability of these neurons to respond to subsequent odors. Combined with the broad tuning of most olfactory neurons (Ma and Shepherd, 2000) and interneuron interactions mediated by extruded potassium ions (Bliss and Rosenberg, 1979) and gaseous messengers (Breer and Shepherd, 1993), ephaptic interactions are evidence against a "dedicated-line" coding mechanism in which a single odorant activates a discrete set of neurons that relay this information to a discrete set of glomeruli in the olfactory bulb (Mombaerts et al., 1996; Treloar et al., 1996). Indeed, this may account for findings that a single odor activates numerous, overlapping populations of glomeruli (Kauer et al., 1987; Johnson et al., 1998; Rubin and Katz, 1999). Counter-intuitively, ephaptic and other interneuronal interactions, by combining the action of broadly tuned neurons, may enhance odor discrimination by integrating these inputs at higher levels of the olfactory system (Pearce et al., 2001).

Furthermore, if olfactory discrimination is dependent on coding expressed by the temporal order of action potentials, ephaptic coupling will influence discrimination by affecting the frequency of action potentials in neighboring axons and by inducing synchrony in their firing (Fig. 3). This synchrony may be involved in generating oscillations in the patterns of input to the olfactory bulb, and these oscillations may be a critical element of the olfactory code (Stopfer et al., 1997). We conclude that the significant effects which ephaptic coupling exerts on activity patterns should be incorporated into any model of olfactory coding and olfactory discrimination.

Densely packed fascicles of unmyelinated axons occur not only in the olfactory nerve but also in diverse structures such as the cerebral cortex, cerebellum, hippocampus, spinal cord, vagus nerve, and peripheral nerves. The present findings suggest that similar ephaptic interactions may occur in these structures and are likely to significantly impact their mechanisms of neuronal integration.

APPENDIX

Mean-field model

The transverse resistance is highest for current flow tangential to the axonal membranes; to estimate its value, we considered paths connecting the spaces around two adjacent axons (Fig. 1*A*). The length of such paths was ~0.5 d, and the cross-sectional area (for a unit length in longitudinal direction) was ~0.05 d, leading to a transverse resistance per unit length $r_t \sim 10\, R_\mathrm{i}$. For $R_\mathrm{i} = 100\ \Omega\mathrm{cm}$, $R_\mathrm{m} = 3333\ \Omega\mathrm{cm}^2$, and $d = 0.2\ \mu\mathrm{m}$, $r_t \sim 0.0001\, r_m$.

Denoting the intracellular potentials of the N_s stimulated and $N - N_s$ unstimulated axons by V_i^A and V_i^B, respectively, and the extracellular potential by V_e, and defining $V^A = V_i^A - V_e - V_{rest}$, $V^B = V_i^B - V_e - V_{rest}$, Ohm's law and current conservation leads to the following cable equations:

$$\frac{1}{r_i}\frac{\partial^2 V_i^A}{\partial x^2} + I_{stim} = i_m^A = c_m\frac{\partial V^A}{\partial t} + I_{ion}^A$$

$$\frac{1}{r_i}\frac{\partial^2 V_i^B}{\partial x^2} = i_m^B = c_m\frac{\partial V^B}{\partial t} + I_{ion}^B$$

$$\frac{1}{r_e}\frac{\partial^2 V_e}{\partial x^2} - I_{stim} = -N_s i_m^A - (N - N_s) i_m^B .$$

For $N_s = 1$, these equations lead to the mean-field equations stated in the text. Note that if there is just one axon in the fascicle, the equations reduce to the standard equations for a single axon enclosed in a thin cytoplasmic sheath (Rall, 1977).

For the passive case with ionic current $I_{ion}^{A,B} = V^{A,B}/r_m$, and $I_{stim} = I\delta(x)$, the solutions of the mean-field equations in the steady state were written as linear superpositions of $exp(-x/\lambda_1)$ and $exp(-x/\lambda_2)$ with $\lambda_1 = \sqrt{\frac{r_m}{r_i}\frac{\beta}{1+\beta}}$ and $\lambda_2 = \sqrt{\frac{r_m}{r_i}}$. For $\beta = 0.05$, $R_\mathrm{i} = 100\ \Omega\mathrm{cm}$, and $R_\mathrm{m} = 3333\ \Omega\mathrm{cm}^2$, $\lambda_1 = 0.0028$ cm and $\lambda_2 = 0.0129$ cm. For active membrane properties, the ionic current is $I_{ion}^{A,B} = g_K(V_i^{A,B} - V_e - E_K) + g_{Na}(V_i^{A,B} - V_e - E_{Na}) + g_L(V_i^{A,B} - V_e - E_L)$, , with $g_K = 36\pi dn^4$ mS/cm, $g_{Na} = 120\pi dm^3 h$ mS/cm, $g_L = 0.3\pi d$ mS/cm, reversal potentials $E_K = V_{rest} - 12$ mV, $E_{Na} = V_{rest} + 115$ mV, $E_L = V_{rest} + 10.613$ mV, and voltage-dependent gating variables are n, m, h, for which evolution is governed by first-order kinetics.

Numerical integration of the equations proceeded with the standard choices for $\Delta x = 0.05\lambda_1,\ 0.1\lambda_1,\ 0.2\lambda_1$, and $\Delta t = 0.2 r_i c_m \Delta x^2$ that are known to be appropriate for Hodgkin–Huxley simulations (de Schutter and Beeman, 1998). We varied the number of compartments between 200 and 1600 in such a way that the physical length of the axons is at least $8\lambda_2$, verifying that the results were virtually indistinguishable for different cases. To ensure that the results were independent of boundary conditions, we ascertained that setting the current flowing through the ends of the axons to zero (sealed end) and setting the membrane

potential at the ends to be at rest gave identical results. We also checked that varying the values of R_i and R_m within the physiological range does not affect the qualitative nature of the results. In all calculations, the specific membrane capacitance $C_m = c_m/\pi d = 1.0\ \mu\text{F/cm}^2$.

Geometric model

The geometric model has 72 potentially distinct membrane potentials and is specified completely by 42 linearly independent coupled partial differential equations (PDEs) and 30 linear constraint equations. However, if only axon A is stimulated, the sixfold symmetry implies that all of the membrane potentials are determined by those of A, *B, C, and D* (Fig. 1*B*). Along with the constraint $V_i^B - V_e^2 - (V_i^B - V_e^3) - (V_i^C - V_e^2) + V_i^C - V_e^3 \equiv 0$ (Fig. 1*B*), this leads to six coupled PDEs for $V_i^A - V_e^1$, $V_i^B - V_e^1$, $V_i^B - V_e^2$, $V_i^C - V_e^2$, $V_i^C - V_e^3$, and $V_i^D - V_e^3$, which we solved for the steady state. We tested two stimulation protocols: (1) current I_{stim} is injected into axon A and $-I_{stim}/24$ is injected into each of the 24 extracellular sites, and (2) current I_{stim} is injected into axon A and $-I_{stim}/6$ is injected into the six extracellular sites immediately around A. The results for the former protocol are virtually indistinguishable from the mean-field calculation; Figure 2, *A* and *B*, depicts results for the latter.

REFERENCES

Barr RC, Plonsey R (1992) Electrophysiological interaction through interstitial space between adjacent unmyelinated parallel fibers. Biophys J 61:1164–1175.

Bliss TVP, Rosenberg ME (1979) Activity-dependent changes in conduction velocity in the olfactory nerve of the tortoise. Pflügers Arch 381:209–216.

Bokil H, Laaris N, Ennis M, Keller A (2001) Ephaptic interactions in the mammalian olfactory bulb. Chem Senses XXIII:129.

Breer H, Shepherd GM (1993) Implications of the NO-cGMP system for olfaction. Trends Neurosci 16:5–9.

Datson MM, Adamek GD, Gesteland RC (1990) Ultrastructural organization of receptor cell axons in frog olfactory nerve. Brain Res 537:69–75.

de Schutter E, Beeman D (1998) Speeding up GENESIS simulations. In: The book of genesis (Bower JM, Beeman D, eds), pp 329–347. New York: Springer.

Doucette JR (1984) The glial cells in the nerve fiber layer of the rat olfactory bulb. Anat Rec 210:385–391.

Duchamp-Viret P, Duchamp A, Chaput MA (2000) Peripheral odor coding in the rat and frog: quality and intensity specification. J Neurosci 20:2383–2390.

Eng DL, Kocsis JD (1987) Activity-dependent changes in extracellular potassium and excitability in turtle olfactory nerve. J Neurophysiol 57:740–754.

Esplin DW (1962) Independence of conduction velocity among myelinated fibers in cat nerve. J Neurophysiol 25:805–811.

Griff ER, Greer CA, Margolis F, Ennis M, Shipley MT (2000) Ultrastructural characteristics and conduction velocity of olfactory receptor neuron axons in the olfactory marker protein-null mouse. Brain Res 866:227–236.

Johnson BA, Woo CC, Leon M (1998) Spatial coding of odorant features in the glomerular layer of the rat olfactory bulb. J Comp Neurol 393:457–471.

Kauer JS, Senseman DM, Cohen LB (1987) Odor-elicited activity monitored simultaneously from 124 regions of the salamander olfactory bulb using a voltage-sensitive dye. Brain Res 418:255–261.

Ma M, Shepherd GM (2000) Functional mosaic organization of mouse olfactory receptor neurons. Proc Natl Acad Sci USA 97:12869–12874.

Malenka RC, Kocsis JD, Ransom BR, Waxman SG (1981) Modulation of parallel fiber excitability by postsynaptically mediated changes in extracellular potassium. Science 214:339–341.

Marín-Padilla M, Amieva MR (1989) Early neurogenesis of mouse olfactory nerve: Golgi and electron microscopic studies. J Comp Neurol 288:339–352.

Mombaerts P, Wang F, Dulac C, Chao SK, Nemes A, Mendelsohn M, Edmondson J, Axel R (1996) Visualizing an olfactory sensory map. Cell 87:675–686.

Moran DT, Rowley JC, Jafek BW, Lovell MA (1982) The fine structure of the olfactory mucosa in man. J Neurocytol 11:721–746.

Pearce TC, Verschure PFMJ, White J, Kauer JS (2001) Robust stimulus encoding in olfactory processing: hyperacuity and efficient signal transmission. In: Emerging computational architectures based on neuroscience (Wermter S, Austin J, Willshaw D, eds), pp 461–480. Heidelberg: Springer.

Poolos NP, Mauk MD, Kocsis JD (1987) Activity-evoked increases in extracellular potassium modulate presynaptic excitability in the CA1 region of the hippocampus. J Neurophysiol 58:404–416.

Press WH, Teukolsky SA, Vellerling WT, Flannery BP (1992) Numerical recipes in C: the art of scientific computing. Cambridge, UK: Cambridge UP.

Rall W (1977) Core conductor theory and cable properties of neurons. In: Handbook of physiology. Section 1, The nervous system. I. Cellular biology of neurons (Kandel ER, Brookhart JM, Mountcastle VB, eds), pp 39–97. Bethesda, MD: American Physiological Society.

Rubin BD, Katz LC (1999) Optical imaging of odorant representations in the mammalian olfactory bulb. Neuron 23:499–511.

Segundo JP (1986) What can neurons do to serve as integrating devices. J Theor Neurobiol 5:1–59.

Stopfer M, Bhagavan S, Smith BH, Laurent G (1997) Impaired odour discrimination on desynchronization of odour-encoding neural assemblies. Nature 390:70–74.

Treloar H, Walters E, Margolis F, Key B (1996) Olfactory glomeruli are innervated by more than one distinct subset of primary sensory olfactory neurons in mice. J Comp Neurol 367:550–562.